OPEN ACCESS
IOP Publishing
Superconductor Science and Technology
Supercond. Sci. Technol. **35** (2022) 105011 (14pp)
https://doi.org/10.1088/1361-6668/ac8e39

Differential geometry method for minimum hard-way bending 3D design of coils with *Re*BCO tape conductor

T H Nes[1,2,*], G de Rijk[3], A Kario[2] and H H J ten Kate[2]

[1] Technology Department, CERN, Meyrin, Switzerland
[2] Faculty of Science and Technology, University of Twente, Enschede, The Netherlands
[3] Retired from Technology Department, CERN, Meyrin, Switzerland

E-mail: t.h.nes@utwente.nl

Received 17 May 2022, revised 19 August 2022
Accepted for publication 31 August 2022
Published 9 September 2022

Abstract

The use of tape conductor poses design challenges for superconducting magnets. Due to its very high aspect ratio, it is hardly possible to bend the conductor over its thin edges (hard-way bending) rather than over its wide side (easy-way bending). Overstraining the conductor causes critical current degradation. In this paper, we propose a new design approach to three-dimensional coil layouts and coil end geometries with tape conductor, which considers the tape's geometrical limitations. To geometrically describe the conductor surface, we use the thin strip model, also referred to as constant perimeter geometry. To prevent conductor degradation, new optimization criteria valid for three-dimensional geometries are presented, which are prevention of conductor creasing, minimization of overall bending energy, and prevention of over-straining the conductor. We will apply this to two 3D coil designs called helix and canted cosine theta. For the design of the coil ends, we propose a new design method using Bézier splines, which allows for much greater design flexibility than previous methods. Two examples of coil end geometries generated with Bézier splines are presented: the so-called cloverleaf and cosine-theta.

Keywords: differential geometry, superconducting magnets, *Re*BCO

(Some figures may appear in colour only in the online journal)

1. Introduction

Tape superconductors, such as *Re*BCO, are increasingly being used in superconducting coils [1–3]. Its very high critical current density allows for the construction of magnets capable of magnetic fields for over 20 T [4]. Generally, bending of the conductor is required in the construction of coils. In magnets with an aperture, the free bore cannot be obstructed by the coil end. In this case, one can use common coil type of magnets, which are double racetracks covering the two magnet apertures [5], or use 3D coil configurations to let the conductor pass over the aperture, such as cloverleaf [6] or saddle coils in a cosine-theta dipole [7] and the MQXF quadrupole [8]. With tape conductors, a 3D configuration creates additional challenges, as thin tapes are very difficult to bend over their thin edges, which is referred to as hard-way or edge-wise bending [9]. This issue must be taken into account when designing the coil geometry. In this paper, we present a mathematical description of the geometry of coils made with *Re*BCO tape conductor, by taking into account its geometric constraints.

* Author to whom any correspondence should be addressed.

For this purpose, we apply differential geometry in the coil design. Previously, authors described the conductor geometry of rectangular conductors, in this case, Rutherford cables, using a mathematical model, referred to as the *thin strip model* [10, 11]. The assumption made in this model is that the conductor can be described as a thin strip surface with zero thickness (infinitely thin) and that the conductor is not bent over its thin edges. The model is also applicable to tape conductor, and we will use it to describe the tape geometry.

For tape conductors, there are, however, additional requirements. In rectangular cables, some edge-wise bending is still possible due to their finite thickness. Tape conductor is much thinner than rectangular cable (around 0.1 mm for tape [12], 1.2–1.5 mm for common Nb_3Sn Rutherford cable [13]), and thus can tolerate much less hard-way bending. Therefore, a different minimization of energy is needed to describe the natural shape of the tape. Another aspect is that overbending of the tape can lead to critical current degradation. In *Re*BCO tapes, critical current degradation occurs due to excessive compressive or tensile strain [12]. The strain distribution in *Re*BCO tapes has been determined by Wang *et al* for the helical and canted cosine theta (CCT) dipole and quadrupole configurations [14]. However, no general relation applicable to any geometry has been investigated yet. Here, we show a general approach, which is applicable to any configuration that can be described by a parametrizable curve of which the curvature and torsion can be determined.

To put the optimization criteria of the coil design into context, we will use them in two geometries frequently used in superconducting coil and cable design called helix and CCT. Helical *Re*BCO windings are used to generate a solenoidal magnetic field in layer-wound solenoids [15, 16], to generate an alternating magnetic field in helical undulators to produce strong radiation in a narrow wavelength range [17], and in superconducting cables such as conductor on round wire (CORC) [18] or high temperature superconductor (HTS) power cables [19]. CCT is a winding configuration that can generate multipole magnetic fields for particle beam steering applications. It was originally proposed in 1969 [20] but has recently become increasingly attractive for various magnet applications, such as dipole magnets for particle accelerators [21], magnets for MRI [22], as well as higher-order magnets, such as quadrupole [23] and combined function magnets [24].

An important issue in the geometric design of the coils is the shape of the coil end. In an accelerator magnet, the coil end goes over the particle beam pipe. Previous design methods of the coil end used polynomial expressions in the description of the shape [10]. However, the polynomial expression requires additional twisting to match the straight section with the coil end, which leads to hard-way bending. In section 5, it will be shown that by using Bézier curves instead of polynomials, this mismatch can be avoided. To demonstrate the versatility of Bézier curves, we will show two examples of accelerator magnet coil end geometries generated with Bézier splines: a cloverleaf coil end and a cosine-theta coil end.

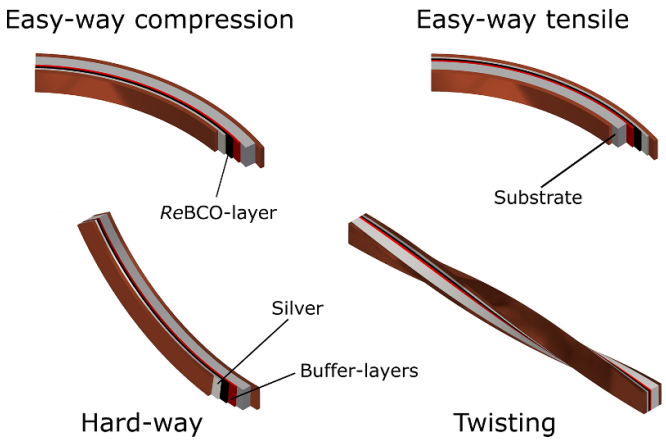

Figure 1. Demonstration of the three types of deformation of a strip-like conductor. Top: easy-way or flat-wise bending, which has the corresponding scalar κ. Bottom left: hard-way or edge-wise bending (κ_g). Bottom right: twisting (τ).

2. Differential geometry in coil design

The basis of modelling strips geometrically starts from a *space* curve $\boldsymbol{r}(t)$, which will be referred to here as the *base* curve of the tape (strip) surface. We refer to it this way, as it is the building block on which the rest of the surface is based. From the base curve, the Frenet–Serret and Darboux apparatus can be derived, which consists of three vectors, ***T, N*** and ***B***, describing the base curve and tape surface, and three scalars for the *normal* curvature κ, *geodesic* curvature κ_g and *torsion* τ. The Frenet–Serret and Darboux equations of differential geometry describe the relation between these scalars and vectors [25, 26].

The scalars κ, κ_g and τ correspond to three different types of deformation of the conductor as shown in figure 1. In easy-way bending, the conductor is bent over the wide side of the conductor. In hard-way bending, the conductor is bent over the thin side of the conductor. When no geodesic curvature is present, a surface is said to be geodesic, and conversely, if geodesic curvature is present the surface is non-geodesic. Lastly, there is twisting, which is the rotation of the conductor along its length.

To describe the tape surface, a *ruler* or *generator* traces out the surface of the tape along the base curve. In figure 2, the principle behind this is shown for a layer jump geometry, which is used for some double coil geometries to connect the top coil to the bottom coil [27]. The direction of the ruler is determined by the rotation of the Frenet–Serret frame along the base curve. The generators are not mere mathematical objects, but can also be seen in real life. In figure 3, an example of this is shown of a copper strip that is bent and twisted.

To describe the perimeter of a hard-way bend free strip, the following equation can be used:

$$\boldsymbol{P}(t) = \boldsymbol{r}(t) \pm \frac{1}{2} g(t) \widehat{\boldsymbol{D}}(t), \tag{1}$$

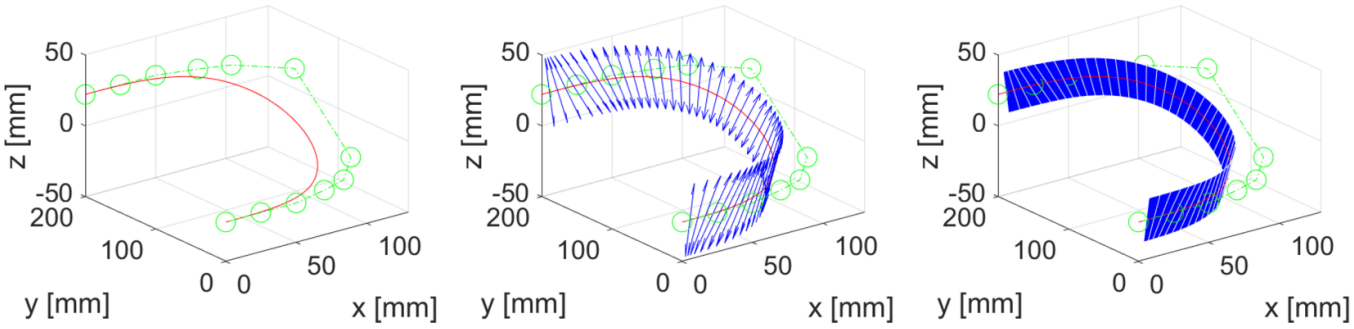

Figure 2. Development of a strip surface from a base curve for a layer jump geometry. On the left, the base curve is plotted. In the middle, the Darboux vectors are calculated from the base curve. On the right, the full strip surface is drawn by choosing the appropriate length of the generators $g(t)$.

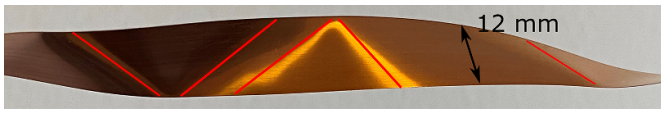

Figure 3. Image of a copper strip, which is being bend and twisted. In the reflection of the light and shadows on the copper strip, the generators can be traced out.

where

$$g(t) = w\sqrt{1+\eta^2},\ \eta = \tau/\kappa, \tag{2}$$

and with the Darboux vector given by:

$$\widehat{\boldsymbol{D}} = \frac{\tau \boldsymbol{T} + \kappa \boldsymbol{B}}{\sqrt{\kappa^2+\tau^2}}. \tag{3}$$

In the language of differential geometry, a surface described by equation (1) is referred to as a *developable surface* or a rectifying *developable*. In magnet design, it is also referred to as a *constant perimeter* geometry [28], as the length of the perimeter of the conductor is conserved under deformation. In appendix A, an overview of the mathematics behind space curves and the Frenet–Serret frame is presented, including a derivation of equation (1).

The thin strip model assumes that the conductor is infinitely thin [10] and does not experience any hard-way bending. In reality, this is of course not the case as tape conductor has a finite thickness, in the case of *Re*BCO it is typically about 0.1 mm and thus hard-way bending is present. In fact, in any twisted tape, with exception of the special case of the helix, hard-way bending is present. The amount of hard way-bending can be expressed as:

$$\kappa_g{}^* = \frac{\lambda\left(\lambda\dot{\kappa}\tau + (1-\lambda\kappa)\,\dot{\tau}\right)}{v\left((1-\lambda\kappa_n)^2 + \lambda^2\tau^2\right)^{3/2}}, \tag{4}$$

where λ is the offset from the base curve. As an example, for a tape conductor, the amount of hard-way bending at the face of the tape is found by using the half-width of the tape for λ, or in the case of two stacked cables λ is the distance between the two cables. A derivation of equation (4) can be found in appendix B. For a thin tape, the hard-way bending can be neglected, as the amount of hard-way bending is proportional to the thickness of the conductor.

Equation (4) implies that for an arbitrary bend and twisted conductor, some hard-way bending is present in the conductor away from the neutral axis. Of interest are the geometries where no hard-way bending is present. In this case, κ_g must be zero. This is true when the numerator in equation (4) equals zero. Omitting the case where $\lambda = 0$, the following relation must hold:

$$\lambda\dot{\kappa}\tau + (1-\lambda\kappa)\,\dot{\tau} = 0. \tag{5}$$

The set of curves that satisfies this equation has common principle normals and are called Bertrand curves. One solution is a planar curve ($\tau = 0$). Another solution is circular helices with constant torsion and curvature ($\dot{\kappa} = \dot{\tau} = 0$). The last possible solution is a skew circle, which has a constant curvature of $\kappa_c = 1/\lambda_c$ and non-zero torsion. This solution is not relevant for coil design, since it only holds for one particular λ. For a conductor of finite thickness, equation (4) implies that under twisting, some hard-way bending is present. The magnitude of this hard-way bending depends on the magnitude of the curvature and twist, the first derivatives, and the thickness of the strip in a non-linear fashion. The thin strip approximation is thus only valid for thin strips, which are not subjected to large changes in curvature and torsion.

Because of equation (4), the only hard-way free coil ends of tape conductor or rectangular cable conductors by which the wide sides do not have a gap between them (excluding geometric defects), are made from planar curves. An example of a planar coil end is a racetrack coil. This is, of course, a very trivial result. More interesting is the fact that there exists no twisted coil end that is hard-way bend free and where the wide sides of the conductor are in full contact. When the second layer is wound on top of the first one, it cannot follow the exact shape unless hard-way bending is allowed.

3. Optimization criteria for tape conductor

3.1. Bending energy

The natural shape of a twisted and bent conductor is the one where its bending energy is minimized. Therefore an

expression of the bending energy is needed such that it can be minimized. For the case of a non-geodesic strip, Wunderlich [29] derived a mathematical expression stating that the total bending energy U can be expressed as a function of normal curvature and torsion:

$$U = \frac{Dw}{2} \int_0^L h(\kappa, \eta, \eta') \, \mathrm{d}s \tag{6}$$

with flexible rigidity:

$$D = \frac{Yd^3}{12(1-\nu^2)}, \tag{7}$$

where Y is the Young's modulus, d the thickness of the strip, ν the Poisson ratio, and:

$$h(\kappa, \eta, \eta') = \kappa^2 \left(1+\eta^2\right)^2 \frac{1}{w\eta'} \ln\left(\frac{2+w\eta'}{2-w\eta'}\right). \tag{8}$$

Equation (7) states that the bending energy is proportional to the thickness of the tape cubed. If we were to bend a *Re*BCO tape of 12 mm wide and 0.1 mm thick over its wide side, it would cost $(12/0.1)^3 = 1.7 \times 10^6$ times more energy to bend compared to bending over its thin side.

3.2. Conductor creasing

In terms of rulers, a local high density of generators means a high bending energy density, and a low generator density a corresponding low bending energy density. Therefore, when two rulers are close to crossing, there is locally an area with a high local bending energy [30]. This can lead to mechanically weak spots in the *Re*BCO. Also, the generator lines should not cross, as this would imply a locally infinite bending energy density and a real physical object cannot be deformed in such a way. With a real physical conductor, trying so would lead instead to creases, damaging it in the process. Thus, when designing a coil geometry, a condition must be made so that in the model the generator lines do not cross. The case where the generators cross is also referred to as *edge of regression* [10, 11]. Therefore, there is a need of an expression stating when the generators cross each other, presented next.

To find the conditions in which this occurs, the following case can be considered (figure 4). Two generators at $\boldsymbol{r}(t)$ and $\boldsymbol{r}(t+\Delta t)$, are separated by a distance Δs. From the point $\boldsymbol{r}(t)$, the perpendicular distance to the perimeter is $w/2$, and the length of the generator at $\boldsymbol{r}(t)$ to one edge of the strip is $\frac{1}{2}w\sqrt{1+\eta^2}$ (see equation (1)). By Pythagoras, the projection of the generators on the baseline is then $w\eta/2$. For the generators not to overlap, the following relation must hold:

$$\Delta s + \frac{w}{2}\eta(t) > \frac{w}{2}\eta(t+\Delta t). \tag{9}$$

As $\Delta s = v\Delta t$, this can be rewritten as:

$$v > \frac{w}{2}\frac{\eta(t+\Delta t) - \eta(t)}{\Delta t}. \tag{10}$$

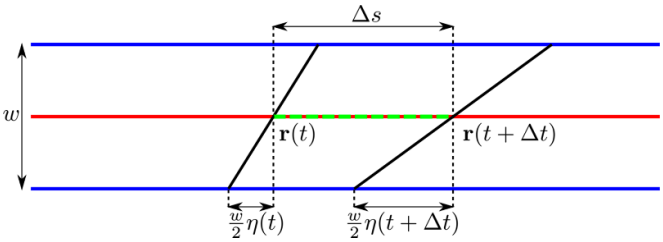

Figure 4. Two generators (black) drawn on the base curve $\boldsymbol{r}(t)$ (red) at positions t and $t+\Delta t$, terminating at the edges of the strip (blue).

Writing this expression in differential notation yields the required condition to prevent generator crossing:

$$\frac{w}{2v}|\dot{\eta}| < 1. \tag{11}$$

The absolute value is taken here to take into consideration the case that the derivative of η is negative, which is the mirrored version of the presented case. We will refer to the term $w|\dot{\eta}|/(2v)$ as the *regression*. From equation (11), it can be seen that in the case of a very wide strip ($w \to \infty$), that η must go to zero to satisfy the relation. This means that it is difficult to twist a strip with a large width without tearing it apart.

If the baseline is chosen at the perimeter of the strip, the condition changes to $w|\dot{\eta}|/v < 1$, because now the full width of the strip must be considered, not the half-width. This has the consequence that the derivative of η can only be half as big compared to a baseline chosen in the centre of the strip for the generators not to cross. Therefore, it is best to choose the baseline in the centre of the strip instead of the perimeter, as this maximizes the allowable $\dot{\eta}$.

3.3. Strain

Besides high local bending energy, *Re*BCO can also be degraded by overstraining. For the two specific cases of the helical and CCT dipole and quadrupole configurations, the strain distribution in *Re*BCO tapes has been determined by Wang *et al* [14]. Here, we will derive a general expression for the strain in the *Re*BCO layer itself under arbitrary bending and twisting.

The most common form of bending is planar bending, i.e. bending along the width of the tape without any torsion present. From figure 5, we can derive that the strain ε is a function of distance from the neutral axis and the local curvature of the neutral axis [31]:

$$\varepsilon = \frac{y}{R}, \tag{12}$$

where y is the distance from the neutral axis, and R is the radius of curvature. When the *Re*BCO layer is not on the neutral axis, the layer is subjected to strain, which can lead to microstructural damage and thus degradation of the critical current of the tape.

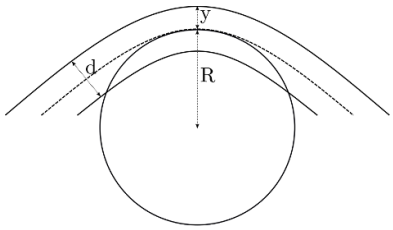

Figure 5. Schematic of the bending of a strip with thickness d. The neutral axis is indicated with the dashed line in the middle of the tape, and the distance from the neutral axis is indicated with y. The bending of the tape can be thought of a local bending over a circle with bending radius R.

For a tape that besides curvature also has torsion, one can use the following reasoning to derive the strain. The generators can be interpreted as the folding lines around the strip, locally each generator can be seen as if the strip is bent around a cylinder. Using the angular velocity relation $v_\perp = \omega \cdot R$, the bending radius can be written as:

$$R = \frac{v_\perp}{\omega} = \frac{v\cos\alpha}{v\sqrt{\kappa^2+\tau^2}}, \tag{13}$$

where ω is the magnitude of the Darboux vector and $v_\perp$ the tangential velocity. Using $\cos\alpha = \kappa/\sqrt{\kappa^2+\tau^2}$ (see appendix A and figure A.3) yields the generalized bending radius, which includes besides the curvature also the torsion:

$$R = \frac{\kappa}{\kappa^2+\tau^2}. \tag{14}$$

Note that for zero torsion the generalized bending radius becomes $R = 1/\kappa$, the planar bending case. Filling this into equation (12) yields the relation between strain, curvature and torsion:

$$\varepsilon = y\frac{\kappa^2+\tau^2}{\kappa}. \tag{15}$$

Van der Laan [32] showed that for *Re*BCO tape, the strain is anisotropic in the *ab*-plane. It is therefore of importance to distinguish the strain along the length (tangential direction) of the tape and the strain along the width (binormal direction) of the tape. In terms of curvature and torsion, the strain along the length of the conductor is:

$$\varepsilon_{\boldsymbol{T}} = \varepsilon\cos\alpha = y\sqrt{\kappa^2+\tau^2}, \tag{16}$$

and the strain along the width of the conductor is:

$$\varepsilon_{\boldsymbol{B}} = \varepsilon\sin\alpha = y\frac{\tau}{\kappa}\sqrt{\kappa^2+\tau^2}. \tag{17}$$

Comparison with measured data of the anisotropic strain dependence of the *Re*BCO conductor in combination with equations (16) and (17) can then be used to optimize the coil design.

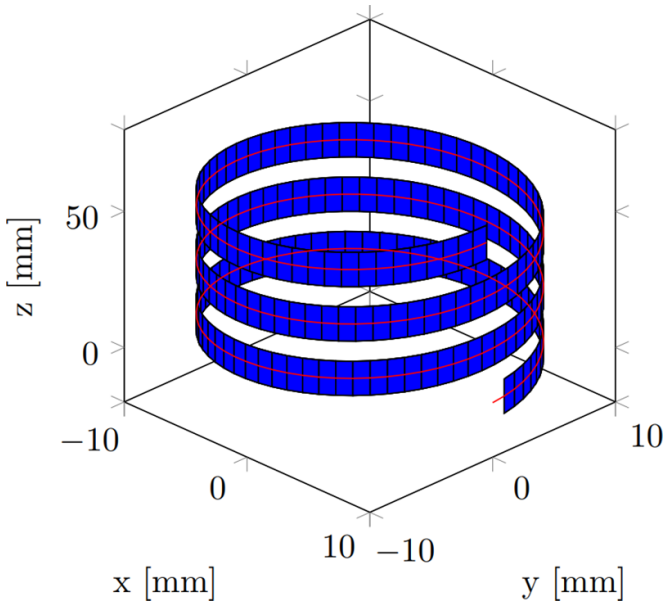

Figure 6. Three turns of a 12 mm wide strip wound in a helical shape with a radius $R = 10$ mm and pitch $p = 20$ mm.

4. Applications to coil and cable design

4.1. Helix

In figure 6, a helical winding made with 12 mm wide strip is shown. Such a helical curve can be parameterized as:

$$\boldsymbol{r}(t) = R\cos t\boldsymbol{e}_x + R\sin t\boldsymbol{e}_y + \frac{p}{2\pi}t\boldsymbol{e}_z, \tag{18}$$

where R is the radius of the cylinder around which the tape is wound and p is the pitch length. Setting $q = p/2\pi$, the Frenet–Serret apparatus can then be found using equations (A.11) and (A.12):

$$\boldsymbol{T} = \frac{-R\sin t\boldsymbol{e}_x + R\cos t\boldsymbol{e}_y + q\boldsymbol{e}_z}{\sqrt{q^2+R^2}}, \tag{19}$$

$$\boldsymbol{B} = \frac{q\sin t\boldsymbol{e}_x - q\cos t\boldsymbol{e}_y + R\boldsymbol{e}_z}{\sqrt{q^2+R^2}}, \tag{20}$$

$$\boldsymbol{N} = -\cos t\boldsymbol{e}_x - \sin t\boldsymbol{e}_y, \tag{21}$$

$$\kappa = \frac{R}{\sqrt{q^2+R^2}}, \tag{22}$$

$$\tau = \frac{q}{\sqrt{q^2+R^2}}. \tag{23}$$

The Darboux vector can be found using equation (A.15):

$$\boldsymbol{D} = \boldsymbol{e}_z. \tag{24}$$

The generators of the helix are thus all pointing in the z-direction, which is along the length of the surface of the cylinder. In the case of the helical parametrization of equation (18), the magnitude of the angular velocity vector is unity.

To find the maximal strain in the *Re*BCO layer, equation (15) can be used. This yields

$$\varepsilon = y\frac{\kappa^2+\tau^2}{\kappa} = \frac{y}{R}. \tag{25}$$

The maximum strain is thus the same as for a tape wound around a cylinder with radius R (equation (12)). The tangential (axial) component of the strain experienced by the *Re*BCO layer is then (equation (16)):

$$\varepsilon_{\boldsymbol{T}} = \frac{y}{\sqrt{q^2+R^2}}, \tag{26}$$

and the binormal (along the width) component (equation (17)):

$$\varepsilon_{\boldsymbol{B}} = \frac{q}{R}\frac{y}{\sqrt{q^2+R^2}}. \tag{27}$$

This is equivalent to the transverse and axial strains found by Wang [14], showing that the generalized expressions for the strain (equations (16) and (17)) yield the same result. The twitch pitch thus influences the relative amount of axial and transverse strain experienced by the *Re*BCO layer. A larger twist pitch yields a proportionally larger transverse strain compared to axial strain. This is important due to the anisotropic dependence of the critical current on the strain. The maximum amount of strain remains proportional to the radius R of the cylinder around it is wound.

4.2. CCT

The base curve of a CCT coil is given by [33]:

$$\boldsymbol{r}(t) = R\cos t\boldsymbol{e}_x + R\sin t\boldsymbol{e}_y + \left(\frac{R\cot\alpha}{n}\sin nt + qt\right)\boldsymbol{e}_z, \tag{28}$$

where R is the radius of the cylinder around the CCT is wound, α the tilt angle, q the pitch, and n the order of the CCT ($n=1$ is a dipole, $n=2$ is a quadrupole etc.). The pitch q can be written as:

$$q = \frac{d_1+d_2}{2\pi\sin\alpha}, \tag{29}$$

where d_1 is the width of the tape and d_2 is the gap between the two tapes in a CCT winding. The curvature and torsion of a CCT winding can be found using equation (A.12), and are:

$$\kappa = \frac{R\sqrt{R^2+\left(q+R\cot\alpha\cos nt\right)^2+n^2R^2\cot^2\alpha\sin^2 nt}}{\left(R^2+\left(q+R\cot\alpha\cos nt\right)^2\right)^{3/2}}, \tag{30}$$

$$\tau = \frac{q+\left(1-n^2\right)\cot\alpha R\cos nt}{R^2+\left(q+R\cot\alpha\cos nt\right)^2+n^2R^2\cot^2\alpha\sin^2 nt}, \tag{31}$$

respectively. The strip surface can then be developed using equation (1). In figure 7, the developed strip surface of five turns of a CCT winding for the first four multi-poles is shown.

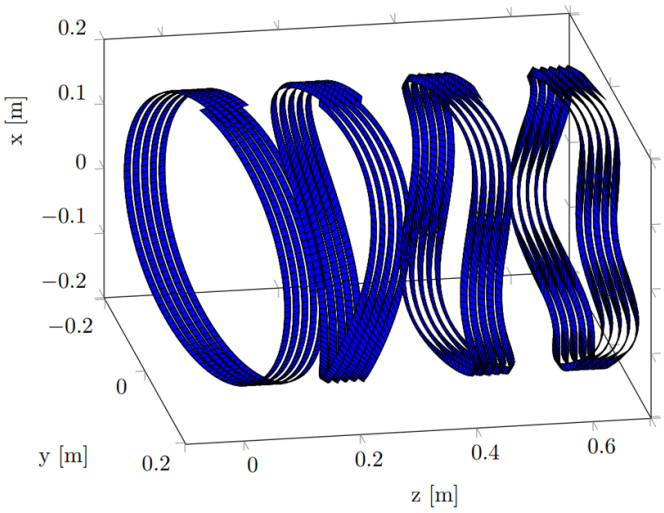

Figure 7. From left to right, five single tape turns of a CCT dipole, quadrupole, sextupole and octupole are shown, with a radius $R = 200$ mm, angle $\alpha = 70°$, strip width $d_1 = 12$ mm and a gap between the tapes $d_2 = 2$ mm.

When designing a CCT configuration with tape conductor like *Re*BCO, it is of importance that the edge of regression condition is not violated, as the crossing of the generators is unphysical and leads to local buckling of the tape, which in the case of *Re*BCO damages the tape. Using that $v(t) = \sqrt{R^2+\left(q+cot\left(\alpha\right)cos\left(nt\right)\right)^2}$, we can verify with the edge of regression condition $d_1|\dot{\eta}|/(2v)<1$ (equation (11)) whether the designed configuration is possible. As an example, three versions of a sextupole CCT winding using tape with a width of 12 mm are shown in figure 8. They have a radius of 100 mm, a gap between the tapes of 1 mm, and have angles α of 20°, 40° and 60° respectively. In figure 11 left, it can be seen that for the cases $\alpha = 20°$ and $\alpha = 40°$, some artefacts in the form of spikes in the modelling occur. This is due to the generators overlapping each other at these points, which is unphysical for a tape. From figure 8 right, it can be seen that for these angles the regression exceeds 1 at these points. It is physically not possible to create a winding with these parameters. If one desires to wind a sextupole with a 12 mm wide tape and a 1 mm gap at these angles, one can increase the radius R, which lowers the regression. For $\alpha = 60°$, the regression remains below 1, and the generators do not overlap.

An expansion to the straight CCT is a curved version. To model the shape with rectangular conductor, it is necessary to know the exact base curve in order to use the thin strip model. One can apply a rotation of the base curve of a straight CCT with a radius r_1 around the origin, which yields:

$$\boldsymbol{r}(t) = \begin{pmatrix} \left(r_1+R\cos t\right)\cos qt - \frac{1}{n}R\cot\alpha\sin nt\sin qt \\ R\sin t \\ \left(r_1+R\cos t\right)\sin qt + \frac{1}{n}R\cot\alpha\sin nt\cos qt \end{pmatrix}, \tag{32}$$

where r_1 is the radius of curvature of the curved CCT. In figure 9, three examples of curved CCT coils made with a single geodesic tape are shown.

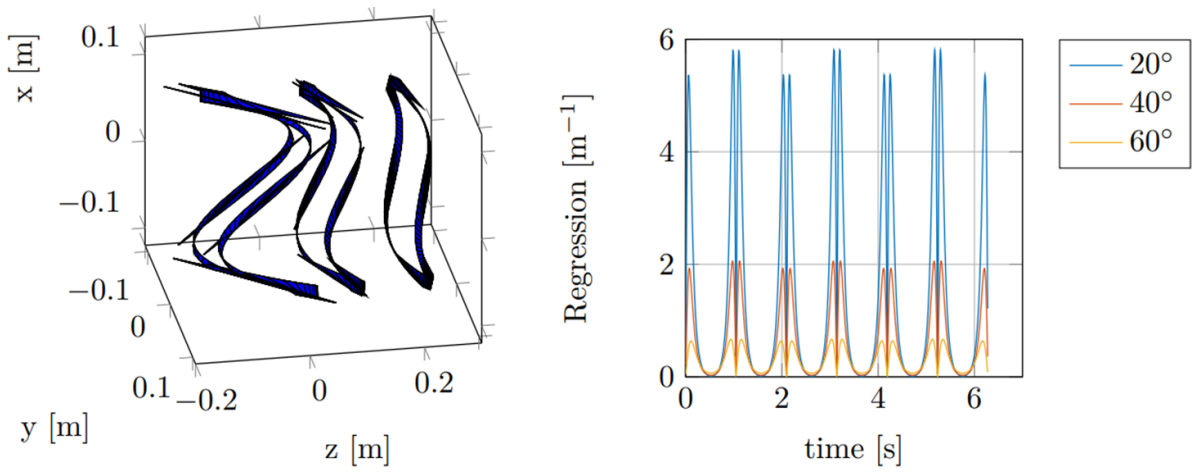

Figure 8. On the left, from left to right three CCT sextupole turns with angles α of 20°, 40° and 60° with radius $R = 100$ mm, width $d_1 = 1$ mm. For the 20° and 40° cases, there are artefacts in the form of spikes present due to the crossing of generators. On the right, the regression is plotted against time. For the 20° and 40° cases, at certain points the regression is larger than 1, meaning that the generators cross and the configuration is not possible to realize physically.

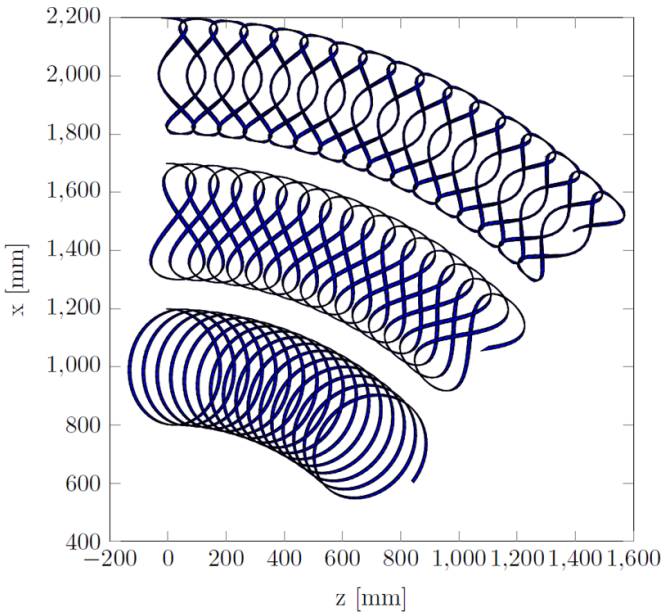

Figure 9. Top-view of a dipole, quadrupole and sextuple curved CCT, made with 12 mm tape. For illustration purposes the distance between each turn d_2 is taken quite large, so that the individual turns are clearly visible.

5. Coil end design using Bézier splines

So far, we have analysed geometries of which the base curve, coil geometry, was already pre-determined. In the coil end of a magnet, this is generally not the case due to the relatively complex shape of the coil end. The geodesic strip description has been used extensively to model magnet coil ends, where the base curve was typically a polynomial expression [10, 11]. Here, we propose to use Bézier splines as a base function. An important advantage of Bézier curves compared to previous design methods relying on polynomials is that they are highly flexible in the shapes that they can create, allowing for great flexibility when creating coil end design. Another advantage is that they allow for the coil end to match the straight section of the magnet without resorting to the need for additional twist, which was required in previous design methods. As additional twist results in additional hard-way bending (equation (A.19)), it must be avoided to minimize the bending energy.

A Bézier curve is a type of parametric curve, defined by a set of control points $\boldsymbol{P}_0$ through $\boldsymbol{P}_n$ in R3, where n is called its order or degree ($n = 1$ for linear, 2 for quadratic, etc.). The Bézier curve is a function of t, defined on the interval $I = [0, 1]$, and can be explicitly expressed as:

$$\boldsymbol{B}(t) = \sum_{k=0}^{n} b_{n,k}(t)\boldsymbol{P}_k, \tag{33}$$

where $b_{n,k}(t)$ are the so-called Bernstein polynomials, defined by:

$$b_{n,k}(t) = \frac{n!}{k!\,(n-k)!}(1-t)^{n-k}t^k. \tag{34}$$

To demonstrate this, we will make use of the property of Bézier curves that the derivative order of the Bézier points at $t = 0$ are proportional to the number of control points [34]. In table 1, the dependence of the first five derivatives of the Bézier curve on the control points at $t = 0$ is tabulated. The first derivative depends on two control points $\boldsymbol{P}_0$ and $\boldsymbol{P}_1$. This means that we are free to choose the location of the other control points $\boldsymbol{P}_3$ to $\boldsymbol{P}_n$ without changing the value of the first derivative. Continuing down the order, the second derivative depends on the first three control points and the third derivative on the first four control points, etc. Similarly, for $t = 1$, the first derivative is proportional to the last two control points ($\boldsymbol{P}_n$ and $\boldsymbol{P}_{n-1}$),

Table 1. Derivatives of a Bézier curve $\boldsymbol{r}(t)$ at $t = 0$. For the derivatives at $t = 1$, all control points $\boldsymbol{P}_i$ get substituted with $\boldsymbol{P}_{n-i}$.

Derivative	Value
$\boldsymbol{r}(0)$	$\boldsymbol{P}_0$
$\frac{d}{dt}\boldsymbol{r}(0)$	$n(\boldsymbol{P}_1 - \boldsymbol{P}_0)$
$\frac{d^2}{dt^2}\boldsymbol{r}(0)$	$n(n-1)(\boldsymbol{P}_2 - 2\boldsymbol{P}_1 + \boldsymbol{P}_0)$
$\frac{d^3}{dt^3}\boldsymbol{r}(0)$	$n(n-1)(n-2)(\boldsymbol{P}_3 - 3\boldsymbol{P}_2 + 3\boldsymbol{P}_1 - \boldsymbol{P}_0)$
$\frac{d^4}{dt^5}\boldsymbol{r}(0)$	$n(n-1)(n-2)(n-3)(\boldsymbol{P}_4 - 4\boldsymbol{P}_3 + 6\boldsymbol{P}_2 - 4\boldsymbol{P}_1 - \boldsymbol{P}_0)$
$\frac{d^5}{dt^5}\boldsymbol{r}(0)$	$n(n-1)(n-2)(n-3)(n-4)(\boldsymbol{P}_5 - 5\boldsymbol{P}_4 + 10\boldsymbol{P}_3 - 10\boldsymbol{P}_2 + 5\boldsymbol{P}_1 - \boldsymbol{P}_0)$

the second derivative is proportional to the last three control points etc.

In the straight section of the coil winding pack, the curvature and torsion are zero. We start by considering the point where the coil end starts, i.e. where $t = 0$. For a continuous transition between the straight section and coil end, we require that the curvature and torsion are both zero at the start of the coil end. We will first set the curvature to zero. For this, it must hold that:

$$\kappa = \frac{\left|\dot{\boldsymbol{r}}(0) \times \ddot{\boldsymbol{r}}(0)\right|}{\left|\dot{\boldsymbol{r}}(0)\right|^3} = 0. \tag{35}$$

This can be achieved if $|\dot{\boldsymbol{r}}(0) \times \ddot{\boldsymbol{r}}(0)| = 0$. From table 1, we can see that if we place the first three control points ($\boldsymbol{P}_0$, $\boldsymbol{P}_1$ and $\boldsymbol{P}_2$) on one line, the cross product will be zero, and hence the curvature is zero as well. As the derivative at $t = 0$ does not depend on the other control points ($\boldsymbol{P}_3 \ldots \boldsymbol{P}_n$), we are still free to move them around, and the curvature remains zero as long as we keep the first three control points fixed on one line. If the first four control points are placed on a line, the first derivative of the curvature is zero. With each extra control point on a line, a higher order of smoothness in curvature is achieved.

Having made the curvature zero at the start point, we will now set the torsion to zero, i.e.:

$$\tau = \frac{(\dot{\boldsymbol{r}}(0) \times \ddot{\boldsymbol{r}}(0))\,\dddot{\boldsymbol{r}}(0)}{|\dot{\boldsymbol{r}}(0) \times \ddot{\boldsymbol{r}}(0)|^2} = 0. \tag{36}$$

However, as $|\dot{\boldsymbol{r}}(0) \times \ddot{\boldsymbol{r}}(0)| = 0$, which was required to get the curvature to zero, the numerator and the denominator are both zero, and we thus get an intermediate form. This can be solved by taking the limit of $t \to 0$, and applying L'Hôpital's rule, which yields:

$$\lim_{t\to 0}\tau(t) = \frac{(\dot{\boldsymbol{r}}(0) \times \dddot{\boldsymbol{r}}(0)) \cdot \frac{d^4}{dt^4}\boldsymbol{r}(0)}{2|\dot{\boldsymbol{r}}(0) \times \dddot{\boldsymbol{r}}(0)|^2} = 0. \tag{37}$$

The torsion is zero when the numerator is zero, which can be achieved when the first five control points $\boldsymbol{P}_0$ to $\boldsymbol{P}_4$ are all in the same plane.

When the curvature and torsion are both zero, the generator length gets ill-defined, as the generator length depends on $\eta = \tau/\kappa$ (equation (2)). The most natural choice is that at the beginning of the coil end, the generator length is equal to the width of the tape, i.e. $\eta(0) = 0$. This requires:

$$\eta(0) = \frac{|\dot{\boldsymbol{r}}(0)|^3 \left(\dot{\boldsymbol{r}}(0) \times \ddot{\boldsymbol{r}}(0)\right) \cdot \dddot{\boldsymbol{r}}(0)}{|\dot{\boldsymbol{r}}(0) \times \ddot{\boldsymbol{r}}(0)|} = 0. \tag{38}$$

As $|\dot{\boldsymbol{r}}(0) \times \ddot{\boldsymbol{r}}(0)| = 0$, we get again an intermediate form. Taking again the limit of $t \to 0$ and applying L'Hôpital's rule yields:

$$\lim_{t\to 0}\eta(t) = |\dot{\boldsymbol{r}}(0)|^3 \frac{(\ddot{\boldsymbol{r}}(0) \times \dddot{\boldsymbol{r}}(0)) \cdot \frac{d^4}{dt^4}\boldsymbol{r}(0) + 2(\dot{\boldsymbol{r}}(0) \times \dddot{\boldsymbol{r}}(0)) \cdot \frac{d^5}{dt^5}\boldsymbol{r}(0)}{6|\dot{\boldsymbol{r}}(0) \times \dddot{\boldsymbol{r}}(0)|^3}. \tag{39}$$

The first part of the numerator is zero due to the requirements on the torsion, where the first five control points are in-plane. The second part of the numerator can be made zero by placing the first six control points in the same plane. For the other side of the coil end (where $t = 1$), also six control points are needed to meet the end of the coil end with a straight section, making for a minimum of twelve control points required. Note that when it is chosen not to make the curvatures match, the total amount of control points for a coil end where torsion is required can be lowered to six. However, a jump in curvature is not ideal from an energy minimizing perspective [35]. An example of a coil end with discontinuous curvature is a racetrack-coil end, where a circle is used to join two straight sections, and the curvature is discontinuous on the joint between the coil end and the straight section.

Using Bézier splines as the base curve for the thin strip model, we can thus model the whole coil end hard-way bend free, and no optimizations are required to minimize the hard-way bending component. For finding the complete minimum bending energy, optimization is still required, as the path the Bézier curve takes must be optimized such that the bending energy given by equation (6H) is minimized. The minimization of the bending energy makes sure that the coil end fits better on a winding mandrel or end spacer.

Bézier splines can be used to create a wide variety of configurations. Here we will show the potential with two examples. In figure 10, a cloverleaf ear made with Bézier splines is shown. Without Bézier splines, it was not possible to create this shape with matching curvature and torsion on the straight section. This ear was used in the design of a cloverleaf type dipole accelerator magnet, which is currently being developed at CERN [6]. This cloverleaf ear has 16 control points in total, which ensures that the transition between the straight section and the ear is smooth in curvature up to the first order.

The development of Bézier splines was originally conceived to make the cloverleaf shape, but can also be used to create other geometries. As an example of this flexibility, in figure 11, a cosine-theta coil end is shown made with Bézier splines. In a cosine-theta coil end, the conductor sits on a cylindrical mandrel and needs to be guided over the beam pipe. In this case, we chose the base curve on the edge of the conductor.

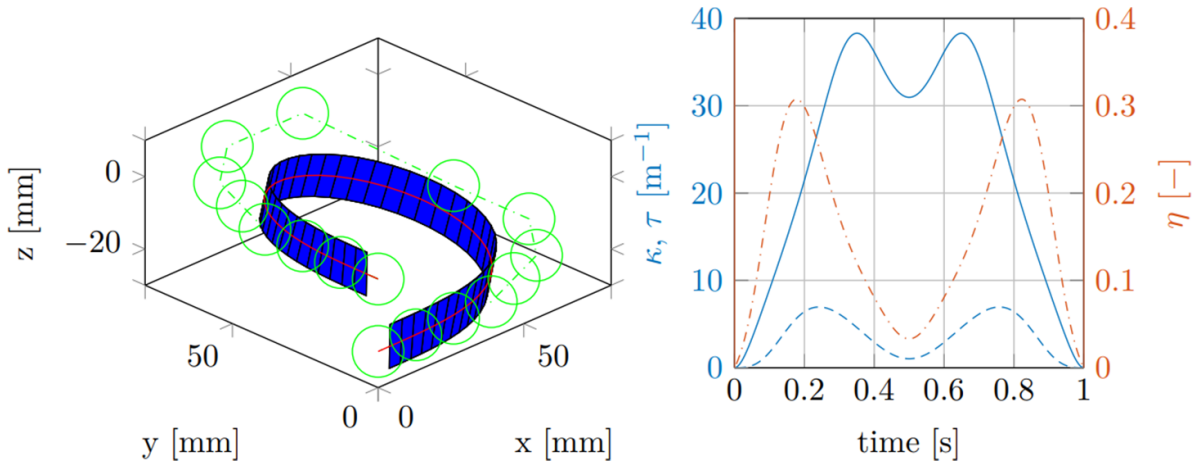

Figure 10. In the left picture, a turn of a cloverleaf ear is shown, made with a Bézier spline with 16 control points. In the right picture, the magnitude of the curvature (solid blue) and torsion (dashed blue) are plotted on the left y-axis, and the magnitude of η (dash dotted red) is plotted on the right y-axis.

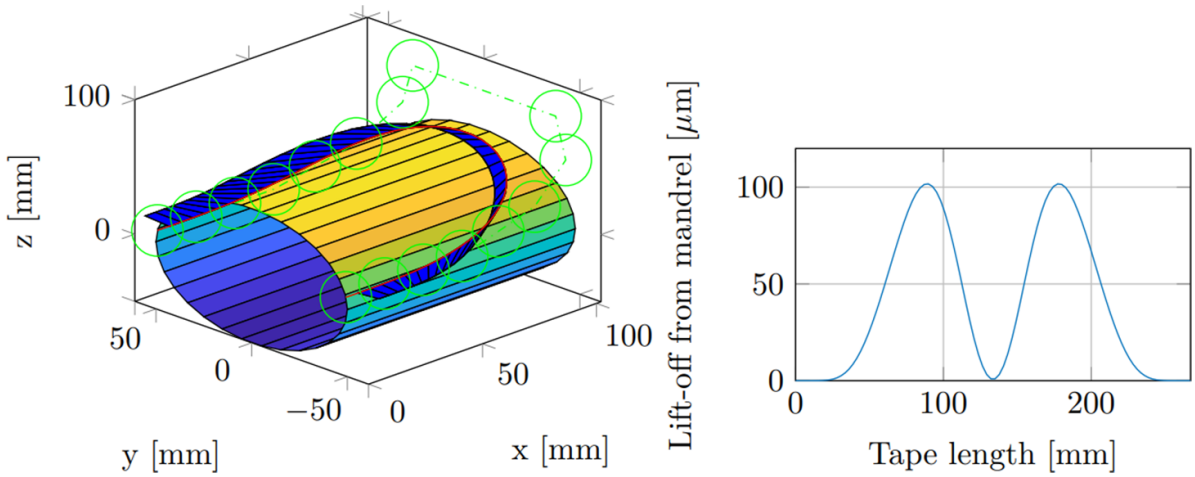

Figure 11. Overview of a cosine-theta coil end designed using Bézier splines. On the left, a plot of the cosine-theta winding is shown. The winding is wound over a cylindrical mandrel. On the right, a plot of the lift-off of the mandrel, i.e. the gap between the tape and the cylindrical mandrel for the created cosine-theta configuration is shown.

The base curve lies not exactly on the cylindrical mandrel but has a small lift off of about 100 μm from the mandrel.

6. Conclusion

In this paper, we have shown how to create coil geometries for tape conductors, such as *Re*BCO coated conductor. This is achieved by the thin strip model, which assumes that the strip is infinitely thin and creates the strip conductor surface by tracing out generators along a base curve. This minimizes the hard-way bending in the strip. The thin strip model is only valid for thin conductors. We have shown mathematically that in stacked cables, hard-way bending is induced when the cables are stacked without a gap in between the turns.

Minimization of the hard-way bending is only one aspect that must be taken into account in the design of coils with *Re*BCO tape conductor. We have shown that for the most mathematically optimal shape, not only the hard-way bending component must be minimized with the thin strip model, but the overall bending energy due to the curvature and torsion has to be minimized as well. This creates geometries with a more natural shape, which is relevant in the design of the coil end. We have derived a mathematical expression for the edge of regression requirement, which states that a coil design is limited by the width of the tape and the ratio of change in curvature and torsion along the conductor length. We have determined expressions for the strain along the length and width of the conductor for generally bent and twisted conductor geometries.

Two examples of applications, the geometry of helical and CCT windings made from tape conductor have been presented. We have derived general expressions for the curvature and strain in a CCT, which can be used to give an estimation of the strain in the CCT turn. Combined with the critical strain of the used *Re*BCO tape in the windings, the coil design can be optimized. Edge of regression violation must be taken into account when designing a CCT. Not all CCT configurations

are possible to create with tape conductor as it is impossible to bend the conductor in such a way that it follows the CCT base curve. Possible ways to alleviate this are using tape with a smaller width or larger tilt angles.

A method to develop coil ends using Bézier splines has been outlined. It can be used to create many diverse coil end geometries that are fully hard-way bend free, and adhere to the boundary conditions imposed by the endpoints. By strategic placement of the control points, the straight section of the magnet can be met without the requirement of additional twist, and edge of regression violations can be prevented. The correct placement of these control points, as well as the minimum number of control points necessary, have been mathematically determined.

The method of Bézier splines in combination with the thin strip model is an improvement to previous methods using polynomials, which are less flexible in their geometric design and cannot meet the straight section without inducing extra hard-way bending.

To demonstrate the usability of Bézier splines, two accelerator dipole coil end configurations made with Bézier splines were presented, the cloverleaf and the cosine-theta. Bézier splines in combination with the thin strip model are thus a powerful tool in the design of coil end geometries with minimized the hard-way bending of *Re*BCO tape conductors.

Data availability statement

No new data were created or analysed in this study.

Acknowledgments

The authors would like to thank Jeroen van Nugteren for his initial work on the cloverleaf geometry, and Stephan Russenschuck for stimulating discussions on the topic.

Appendix A. Thin strip model

A.1. Space curves

A space curve is a curve that 'lives' in a three-dimensional Euclidian space $\boldsymbol{R}^3$, as opposed to a plane curve, which lives in $\boldsymbol{R}^2$. It is a very general form of a curve. To model strip surfaces, only real, differentiable curves are of interest. For a rigorous mathematical description of space curves, the reader is referred to elementary works on differential geometry [25, 26]. The trace of a space curve can be given by the locus of the position vector $\boldsymbol{r}(t)$, which is a smooth, parametrizable function of the real parameter t with a parameter space interval $I = [a,b] \subset \boldsymbol{R}$, where a and b are the start and endpoints of the interval respectively. Introducing a Cartesian coordinate system, $\boldsymbol{r}(t)$ can be written as:

$$\boldsymbol{r}(t) = x(t)\,\boldsymbol{e}_x + y(t)\,\boldsymbol{e}_y + z(t)\,\boldsymbol{e}_z. \tag{A.1}$$

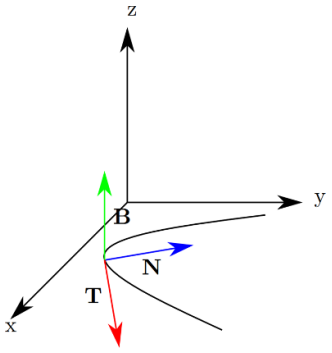

Figure A1. Image of a space curve sitting in the xy-plane, with the Frenet–Serret frame consisting of the vectors $\boldsymbol{T}$, $\boldsymbol{N}$, and $\boldsymbol{B}$. The vector $\boldsymbol{T}$ lies tangential to the curve, the vector $\boldsymbol{N}$ normal to the curve and the vector $\boldsymbol{B}$ is orthogonal to both.

If t changes in the interval I, the tangent of the space curve is the derivative $\mathrm{d}\boldsymbol{r}/\mathrm{d}t$ at $\boldsymbol{r}(t)$. If the parameter t is interpreted as the time, then the tangent vector can be seen as the velocity $\dot{\boldsymbol{r}}(t) = \boldsymbol{v}(t)$, where the dot refers to the t-derivative. The tangent vector $\boldsymbol{T}(t)$ is the unit vector that is tangent to a curve (or surface) at any given point. It is defined as the unit vector in the direction of $\boldsymbol{v}(t)$:

$$\boldsymbol{T}(t) = \frac{\boldsymbol{v}(t)}{v(t)}, \tag{A.2}$$

with $v(t) = |\boldsymbol{v}(t)|$.

The arc length of a space curve traced out by $\boldsymbol{r}(t)$ from the point $t_0 \in I$, is by definition:

$$s(t) = \int_{t_0}^{t} \left|\dot{\boldsymbol{r}}(t)\right| \mathrm{d}t. \tag{A.3}$$

Since differentiable curves are assumed ($v(t) \neq 0$), the arc length s is a differentiable function of t and $\mathrm{d}s/\mathrm{d}t = v(t)$. One can switch between parametrization with parameter t and arc-length parameter s using $\mathrm{d}/\mathrm{d}s = 1/v \bullet \mathrm{d}/\mathrm{d}t$. If the curve is of unit velocity, the curve is said to be arc-length parameterized with respect to parameter t, since $\mathrm{d}s = \mathrm{d}t$. Using unit-speed curves would seem more natural in our case, as we are not dealing with a kinematic object, but a geometric object in which terms such as velocity and time are not relevant. In principle, it is always possible to generate a unit-speed curve from a non-unit speed curve with the same trace by normalizing the velocity in equation (A.3) and integrate it. However, it is often hard or impossible to find the anti-derivative, which makes the procedure of producing a unit-speed parametrization of a curve rather difficult in general. Therefore, for practical reasons, we will use the general case of a non-unit speed curve, unless it is part of a definition.

A.2. The Frenet–Serret frame

A space curve only describes a line on the surface of the strip following the tangential direction. The conductor also has a width and a normal perpendicular to the tape surface. Here,

we will assign a frame to the space curve, which consists of the tangential vector $\boldsymbol{T}$, normal vector $\boldsymbol{N}$ and binormal vector $\boldsymbol{B}$. We will use these vectors to assign a normal direction pointing perpendicular to the tape surface and a binormal direction pointing in the direction of the tape width.

We will consider a regular arc-length parameterized curve. Since the tangent vector is a unit vector, it is normal to its s-derivative. This can be seen by considering the relation $\boldsymbol{T}(s) \bullet \boldsymbol{T}(s) = 1$, and differentiating this relation which gives $2\boldsymbol{T}(s) \bullet \boldsymbol{T}'(s) = 0$. The prime refers to taking the s-derivative. By normalizing this vector, we define the unit principle normal vector $\boldsymbol{N}(s)$ as:

$$\boldsymbol{N}(s) = \frac{\boldsymbol{T}'(s)}{\left|\boldsymbol{T}'(s)\right|}. \tag{A.4}$$

The absolute value of the vector $\boldsymbol{T}'(s)$ and its inverse:

$$\kappa(s) = \left|\boldsymbol{T}'(s)\right|, \ \rho(s) = 1/\kappa(s), \tag{A.5}$$

are called the curvature of the curve and radius of curvature respectively. We can interpret the curvature as the failure of the curve being a straight line. The vector:

$$\boldsymbol{B}(s) = \boldsymbol{T}(s) \times \boldsymbol{N}(s), \tag{A.6}$$

is called the unit binormal vector. Taking the s-derivative gives:

$$\begin{aligned}\boldsymbol{B}'(s) &= (\boldsymbol{T}(s) \times \boldsymbol{N}(s))' = \boldsymbol{T}'(s) \times \boldsymbol{N}(s) + \boldsymbol{T}(s) \times \boldsymbol{N}'(s) \\ &= \kappa \boldsymbol{N}(s) \times \boldsymbol{N}(s) + \boldsymbol{T}(s) \times \boldsymbol{N}'(s) = \boldsymbol{T}(s) \times \boldsymbol{N}'(s).\end{aligned} \tag{A.7}$$

As $\boldsymbol{B}(s)$ is a unit vector, it is again normal to its s-derivative, and since it is also orthogonal to $\boldsymbol{T}(s)$ (equation (A.6)), a similar relation to equation (A.4) holds:

$$\boldsymbol{N}(s) = \frac{\boldsymbol{B}'(s)}{\left|\boldsymbol{B}'(s)\right|}. \tag{A.8}$$

The absolute value of the vector $\boldsymbol{B}'(s)$ and its inverse:

$$\tau(s) = -\left|\boldsymbol{B}'(s)\right|, \ \sigma(s) = 1/\tau(s), \tag{A.9}$$

are called the torsion of the curve and the radius of torsion respectively. We can interpret the torsion as a measurement of the failure of the curve to remain in-plane. The minus sign is there so that a positive torsion corresponds to an upward motion with respect to the plane.

The vectors $\boldsymbol{T}$, $\boldsymbol{N}$ and $\boldsymbol{B}$, collectively called the Frenet–Serret frame, form an orthonormal basis spanning $\boldsymbol{R}^3$. The relations between the Frenet–Serret frame at s and $s + \mathrm{d}s$ are given by the Frenet–Serret equations:

$$\begin{aligned}&\frac{\mathrm{d}\boldsymbol{T}(s)}{\mathrm{d}s} = \kappa(s)\boldsymbol{N}(s), \ \frac{\mathrm{d}\boldsymbol{N}(s)}{\mathrm{d}s} = \tau(s)\boldsymbol{B}(s) - \kappa(s)\boldsymbol{T}(s) \\ &\frac{\mathrm{d}\boldsymbol{B}(s)}{\mathrm{d}s} = -\tau(s)\boldsymbol{N}(s).\end{aligned} \tag{A.10}$$

The collection of $\boldsymbol{T}$, $\boldsymbol{N}$, $\boldsymbol{B}$, κ and τ is called the Frenet–Serret apparatus. In terms of a space curve with parameter t, it can be shown that the Frenet–Serret frame is given by:

$$\boldsymbol{T} = \frac{\dot{\boldsymbol{r}}(t)}{|\dot{\boldsymbol{r}}(t)|}, \ \boldsymbol{N} = \boldsymbol{B} \times \boldsymbol{T}, \ \boldsymbol{B} = \frac{\dot{\boldsymbol{r}}(t) \times \ddot{\boldsymbol{r}}(t)}{|\dot{\boldsymbol{r}}(t) \times \ddot{\boldsymbol{r}}(t)|}, \tag{A.11}$$

and the curvature and torsion are given by:

$$\kappa = \frac{|\dot{\boldsymbol{r}}(t) \times \ddot{\boldsymbol{r}}(t)|}{|\dot{\boldsymbol{r}}(t)|^3}, \ \tau = \frac{(\dot{\boldsymbol{r}}(t) \times \ddot{\boldsymbol{r}}(t)) \cdot \dddot{\boldsymbol{r}}(t)}{|\dot{\boldsymbol{r}}(t) \times \ddot{\boldsymbol{r}}(t)|^2}. \tag{A.12}$$

In figure (A1), a space curve with its Frenet-Serret frame is shown. The Frenet–Serret equations in terms of a parameter t are in matrix form:

$$\begin{pmatrix} \dot{\boldsymbol{T}} \\ \dot{\boldsymbol{N}} \\ \dot{\boldsymbol{B}} \end{pmatrix} = v \begin{pmatrix} 0 & \kappa & 0 \\ -\kappa & 0 & \tau \\ 0 & -\tau & 0 \end{pmatrix} \begin{pmatrix} \boldsymbol{T} \\ \boldsymbol{N} \\ \boldsymbol{B} \end{pmatrix}. \tag{A.13}$$

Since the matrix in equation (A.13) is a skew-symmetric matrix, the Frenet–Serret equations can be written as a cross-product:

$$\begin{pmatrix} \dot{\boldsymbol{T}} \\ \dot{\boldsymbol{N}} \\ \dot{\boldsymbol{B}} \end{pmatrix} = \begin{pmatrix} v\tau\boldsymbol{T} \\ 0 \\ v\kappa\boldsymbol{B} \end{pmatrix} \times \begin{pmatrix} \boldsymbol{T} \\ \boldsymbol{N} \\ \boldsymbol{B} \end{pmatrix}. \tag{A.14}$$

The vector in front of the cross product is the angular velocity vector of the Frenet–Serret frame. Its direction determines the moving frame's momentary axis of motion (its centrode) and its magnitude the angular speed. It can thus be written as:

$$\boldsymbol{D} = v(\tau\boldsymbol{T} + \kappa\boldsymbol{B}). \tag{A.15}$$

The angular velocity vector is also known as the Darboux vector. We can find the direction of the Darboux vector by normalization:

$$\widehat{\boldsymbol{D}} = \frac{\tau\boldsymbol{T} + \kappa\boldsymbol{B}}{\sqrt{\kappa^2 + \tau^2}}. \tag{A.16}$$

As with space curves, strips also have an orthonormal frame associated with them. The tangent vector of the strip $\boldsymbol{t}$ points in the direction of the base curve, and the normal vector $\boldsymbol{n}$ is directed normal to the surface. The binormal vector $\boldsymbol{b}$ is orthonormal to both these vectors. The set $\boldsymbol{t}$, $\boldsymbol{n}$, $\boldsymbol{b}$ forms the frame for strips (see figure (A2)). This frame is called the Darboux frame. To find the Darboux frame, the Frenet–Serret frame can be rotated with an angle φ around the tangent vector, such that the normal vector $\boldsymbol{N}$ aligns with the normal vector $\boldsymbol{n}$ of the space curve:

$$\begin{pmatrix} \boldsymbol{t} \\ \boldsymbol{n} \\ \boldsymbol{b} \end{pmatrix} = \begin{pmatrix} 1 & 0 & 0 \\ 0 & \cos\varphi & \sin\varphi \\ 0 & -\sin\varphi & \cos\varphi \end{pmatrix} \begin{pmatrix} \boldsymbol{T} \\ \boldsymbol{N} \\ \boldsymbol{B} \end{pmatrix}. \tag{A.17}$$

Taking the derivative of the previous equation, and using its inverse and the Frenet–Serret equations, yields:

$$\begin{pmatrix} \dot{\boldsymbol{t}} \\ \dot{\boldsymbol{n}} \\ \dot{\boldsymbol{b}} \end{pmatrix} = v \begin{pmatrix} 0 & \kappa_{\mathrm{n}} & -\kappa_{\mathrm{g}} \\ -\kappa_{\mathrm{n}} & 0 & \tau_{\mathrm{r}} \\ \kappa_{\mathrm{g}} & -\tau_{\mathrm{r}} & 0 \end{pmatrix} \begin{pmatrix} \boldsymbol{t} \\ \boldsymbol{n} \\ \boldsymbol{b} \end{pmatrix}, \tag{A.18}$$

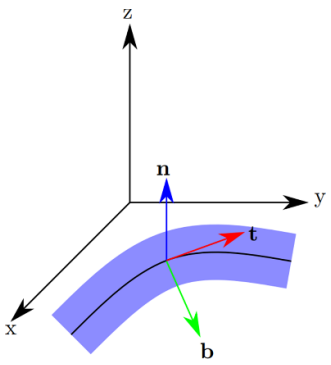

Figure A2. Image of a non-geodesic strip sitting in the *xy*-plane, with the Darboux frame consisting of the vectors ***t, n***, and ***b***. The vector ***t*** lies tangential to the strip, the vector ***n*** normal to the strip surface and the vector ***b*** lies along the width of the strip surface.

where τ_{r} is the geodesic torsion, κ_{g} the geodesic curvature, and κ_{n} the normal curvature, which are expressed in terms of curvature and torsion:

$$\tau_{\mathrm{r}} = \tau + \varphi', \ \kappa_{\mathrm{g}} = \kappa \sin\varphi, \ \kappa_{\mathrm{n}} = \kappa \cos\varphi. \tag{A.19}$$

For our conductor, we assume that no hard-way bending is present, which means that there is no geodesic curvature ($\kappa_{\mathrm{g}} = 0$). In this case, the Darboux apparatus is equal to the Frenet–Serret apparatus.

Analogous to equation (A.14), we can write equation (A.18) as a cross product:

$$\begin{pmatrix} \dot{\boldsymbol{t}} \\ \dot{\boldsymbol{n}} \\ \dot{\boldsymbol{b}} \end{pmatrix} = \begin{pmatrix} v\tau_{\mathrm{r}}\boldsymbol{t} \\ v\kappa_{\mathrm{g}}\boldsymbol{n} \\ v\kappa_{\mathrm{n}}\boldsymbol{b} \end{pmatrix} \times \begin{pmatrix} \boldsymbol{t} \\ \boldsymbol{n} \\ \boldsymbol{b} \end{pmatrix}, \tag{A.20}$$

and we can define an angular velocity vector:

$$\boldsymbol{\omega} = v\left(\tau_{\mathrm{r}}\boldsymbol{T} + \kappa_{\mathrm{g}}\boldsymbol{N} + \kappa_{\mathrm{n}}\boldsymbol{B}\right). \tag{A.21}$$

We can link this to the three deformation modes of a tape conductor (figure 1). The term $v\tau_{\mathrm{r}}$ is the rotation around the tangent vector (twisting), $v\kappa_{\mathrm{g}}$ the rotation around the normal vector (hard-way bending) and $v\kappa_{\mathrm{n}}$ the rotation around the binormal vector (easy-way bending).

A.3. Modelling the strip surface

By moving a line $\boldsymbol{g}(t)$ (called a generator) along a curve $\boldsymbol{r}(t)$, one can trace out the surface $\boldsymbol{S}$ of a strip. A surface like this is called a *ruled* surface. It can be written down parametrically as:

$$\boldsymbol{S}(t) = \boldsymbol{r}(t) + \boldsymbol{g}(t), \tag{A.22}$$

where $\boldsymbol{r}(t)$ is the base curve (also called directrix) of the representation, and $\boldsymbol{g}(t)$ the generator, with $g(t)$ the length of the generator and $\widehat{\boldsymbol{g}}(t)$ the direction of the generator.

A *developable* surface is a special kind of ruled surface. It is a surface which can be created by transforming a plane, for instance by folding and bending, but not by stretching or compression. Conversely, a developable surface can be flattened on a plane without stretching or compressing it. Such a surface is comparable to bending a thin paper strip, without tearing or creasing it. These properties are also the same for the conductor we want to model: we can bend it, but we cannot crease or tear it. Hence we will use a developable surface to model the conductor.

One can show that for a ruled surface to be a developable surface, the following relation must hold [25]:

$$\det\left(\dot{\boldsymbol{r}}, \boldsymbol{g}, \dot{\boldsymbol{g}}\right) = 0. \tag{A.23}$$

Since for a geodesic strip the Frenet–Serret frame is equal to the Darboux frame, the generator lies in the plane spanned by $\boldsymbol{T}$ and $\boldsymbol{B}$, i.e. a linear combination of $\boldsymbol{T}$ and $\boldsymbol{B}$:

$$\boldsymbol{g} = \zeta\boldsymbol{T} + \xi\boldsymbol{B}. \tag{A.24}$$

Differentiating yields:

$$\dot{\boldsymbol{g}} = \dot{\zeta}\boldsymbol{T} + v(\zeta\kappa - \xi\tau)\boldsymbol{N} + \dot{\xi}\boldsymbol{B}. \tag{A.25}$$

From equation (A.23), the surface is developable when the following determinant is zero:

$$\det\begin{pmatrix} 1 & \zeta & \dot{\zeta} \\ 0 & 0 & v(\zeta\kappa - \xi\tau) \\ 0 & \xi & \dot{\xi} \end{pmatrix} = -\xi v(\zeta\kappa - \xi\tau) = 0. \tag{A.26}$$

This determinant is zero when $\zeta = c\tau$ and $\xi = c\kappa$, where c is a function depending on t. The generator is then:

$$\boldsymbol{g}(t) = c(\tau\boldsymbol{T} + \kappa\boldsymbol{B}). \tag{A.27}$$

The part between brackets is equal to the Darboux vector (barring a factor v). The direction of the generator is thus given by the (normalized) Darboux vector ($\widehat{\boldsymbol{g}}(t) = \widehat{\boldsymbol{D}}(t)$), and we can write equation (A.27) as:

$$\boldsymbol{g}(t) = g(t)\widehat{\boldsymbol{D}}(t), \tag{A.28}$$

where $g(t) = c(t)\sqrt{\kappa^2 + \tau^2}$. The generator length must have a specific length such that the width of the tape remains the same everywhere along the curve. The magnitude of the generator length can be determined by comparing the two triangles in figure (A3). As the Darboux vector points in the direction of the generator, and the binormal vector in the direction perpendicular to the edges of the strip, the triangles are congruent: the angle α is the same in both triangles:

$$\tan\alpha = \frac{\tau}{\kappa}, \ \cos\alpha = \frac{w}{g}. \tag{A.29}$$

Rearranging these two expressions yields the expression for g(t):

$$g(t) = w\sqrt{1 + \eta^2}, \tag{A.30}$$

where $\eta = \tau/\kappa$.

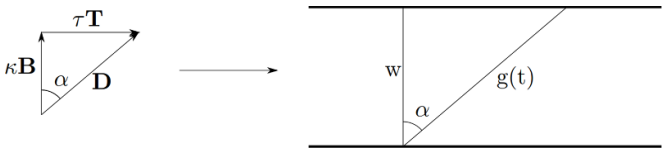

Figure A3. Determination of the generator length. On the left is the triangle formed by the Darboux vector and its Frenet–Serret components, on the right is drawn the tape surface with tape width w and generator length $g(t)$.

To make a drawing of the surface, we need to know the location of the perimeters of the tape. This can be done by drawing the generators on the base curve and connecting the top and the bottom of successive generators, which will form the perimeter $\boldsymbol{P}(t)$ of the tape:

$$\boldsymbol{P}(t) = \boldsymbol{r}(t) \pm \frac{1}{2} g(t) \widehat{\boldsymbol{D}}(t). \tag{A.31}$$

Appendix B. Extension to conductor with a finite thickness

The thin strip model assumes that the conductor is infinitely thin. However, a real conductor has a finite thickness. Also in the coil end, the conductors are generally stacked on top of each other. To look at the effect of the finite thickness, we will look at a surface, which is offset from the thin strip surface in the normal direction (figure A4).

The parallel curve can be parameterized as:

$$\boldsymbol{r}^*(t) = \boldsymbol{r}(t) + \lambda \boldsymbol{N}(t). \tag{B.1}$$

Differentiating with respect to t yields:

$$\frac{\mathrm{d}\boldsymbol{r}^*(t)}{\mathrm{d}t} = \frac{\mathrm{d}\boldsymbol{r}(t)}{\mathrm{d}t} + \lambda \frac{\mathrm{d}\boldsymbol{N}(t)}{\mathrm{d}t}, \tag{B.2}$$

which is in turns of velocity:

$$\boldsymbol{v}^*(t) = v\left((1-\lambda\kappa)\boldsymbol{T} + \lambda\tau\boldsymbol{B}\right). \tag{B.3}$$

The magnitude of the velocity of the parallel curve is then:

$$v^* = v\sqrt{(1-\lambda\kappa)^2 + \lambda^2\tau^2}. \tag{B.4}$$

The unit tangent vector of the parallel frame is then:

$$\boldsymbol{t}^*(t) = \frac{\boldsymbol{v}^*}{v} = \frac{(1-\lambda\kappa_\mathrm{n})\boldsymbol{T} + \lambda\tau\boldsymbol{B}}{\sqrt{(1-\lambda\kappa_\mathrm{n})^2 + \lambda^2\tau^2}}. \tag{B.5}$$

The normal vector of the parallel strip must be equal to the normal vector of the base curve:

$$\boldsymbol{n}^*(t) = \boldsymbol{N}(t). \tag{B.6}$$

The unit binormal vector is then:

$$\boldsymbol{b}^*(t) = \frac{(1-\lambda\kappa_\mathrm{n})\boldsymbol{B} - \lambda\tau\boldsymbol{T}}{\sqrt{(1-\lambda\kappa_\mathrm{n})^2 + \lambda^2\tau^2}}. \tag{B.7}$$

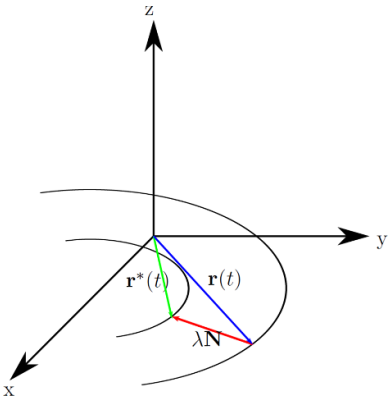

Figure A4. Drawing of a parallel curve $\boldsymbol{r}^*(t)$ by offsetting the curve $\boldsymbol{r}$ in the normal direction $\boldsymbol{N}$ with a distance λ.

The set $\{\boldsymbol{t}^*, \boldsymbol{n}^*, \boldsymbol{b}^*\}$ forms the Darboux frame of the parallel curve. In matrix form it is written as:

$$\begin{pmatrix} \boldsymbol{t}^* \\ \boldsymbol{n}^* \\ \boldsymbol{b}^* \end{pmatrix} = \begin{pmatrix} \frac{1-\lambda\kappa_\mathrm{n}}{\sqrt{(1-\lambda\kappa_\mathrm{n})^2+\lambda^2\tau^2}} & 0 & \frac{\lambda\tau}{\sqrt{(1-\lambda\kappa_\mathrm{n})^2+\lambda^2\tau^2}} \\ 0 & 1 & 0 \\ -\frac{\lambda\tau}{\sqrt{(1-\lambda\kappa_\mathrm{n})^2+\lambda^2\tau^2}} & 0 & \frac{1-\lambda\kappa_\mathrm{n}}{\sqrt{(1-\lambda\kappa_\mathrm{n})^2+\lambda^2\tau^2}} \end{pmatrix} \times \begin{pmatrix} \boldsymbol{T} \\ \boldsymbol{N} \\ \boldsymbol{B} \end{pmatrix}. \tag{B.8}$$

Taking the derivative with respect to t yields:

$$\begin{pmatrix} \dot{\boldsymbol{t}}^* \\ \dot{\boldsymbol{n}}^* \\ \dot{\boldsymbol{b}}^* \end{pmatrix} = v^* \begin{pmatrix} 0 & {\kappa_\mathrm{n}}^* & -{\kappa_\mathrm{g}}^* \\ -{\kappa_\mathrm{n}}^* & 0 & {\tau_\mathrm{r}}^* \\ {\kappa_\mathrm{g}}^* & -{\tau_\mathrm{r}}^* & 0 \end{pmatrix} \begin{pmatrix} \boldsymbol{t}^* \\ \boldsymbol{n}^* \\ \boldsymbol{b}^* \end{pmatrix}, \tag{B.9}$$

where the parallel relative torsion, geodesic curvature and normal curvature are:

$${\tau_\mathrm{r}}^* = \frac{\tau}{(1-\lambda\kappa_\mathrm{n})^2 + \lambda^2\tau^2}, \tag{B.10}$$

$${\kappa_\mathrm{g}}^* = \frac{\lambda\left(\lambda\dot{\kappa}\tau + (1-\lambda\kappa)\dot{\tau}\right)}{v\left((1-\lambda\kappa_\mathrm{n})^2 + \lambda^2\tau^2\right)^{3/2}}, \tag{B.11}$$

$${\kappa_\mathrm{n}}^* = \frac{\kappa + \lambda\left(\kappa^2+\tau^2\right)}{(1-\lambda\kappa_\mathrm{n})^2 + \lambda^2\tau^2}, \tag{B.12}$$

respectively.

ORCID iDs

T H Nes https://orcid.org/0000-0002-9241-7190
H H J ten Kate https://orcid.org/0000-0001-5597-3190

References

[1] Rossi L and Senatore C 2021 HTS accelerator magnet and conductor development in Europe *Instruments* **5** 8

[2] Bai H *et al* 2020 The 40 T superconducting magnet project at the national high magnetic field laboratory *IEEE Trans. Appl. Supercond.* **30** 4300405

[3] van der Laan D *et al* 2020 A CORC® cable insert solenoid: the first high-temperature superconducting insert magnet tested at currents exceeding 4 kA in 14 T background magnetic field *Supercond. Sci. Technol.* **33** 074002

[4] van Nugteren J, Kirby G, Murtomäki J, De Rijk G, Rossi L and Stenvall A 2018 Toward REBCO 20 T+ dipoles for accelerators *IEEE Trans. Appl. Supercond.* **28** 4008509

[5] Gupta R *et al* 2017 Common coil dipoles for future high energy colliders *IEEE Trans. Appl. Supercond.* **27** 4000605

[6] Nes T H, Kirby G, de Rijk G, Canale M, Gentini L, van Nugteren J, Kario A and ten Kate H H J 2022 Design of a cloverleaf-racetrack dipole demonstrator magnet with dual ReBCO conductor *IEEE Trans. Appl. Supercond.* **32** 4002105

[7] Valente R U *et al* 2021 Study of superconducting magnetization effects and 3D electromagnetic analysis of the Nb_3Sn cosθ short model for FCC *IEEE Trans. Appl. Supercond.* **31** 4002205

[8] Yu M, Ambrosio G, Izquierdo Bermudez S, Bossert R, Brandt J, Ferracin P and Krave S 2017 Coil end parts development using bend and design for MQXF by LARP *IEEE Trans. Appl. Supercond.* **27** 4000105

[9] Kajita K, Takao T, Maeda H and Yanagisawa Y 2017 Degradation of a REBCO conductor due to an axial tensile stress under edgewise bending: a major stress mode of deterioration in a high field REBCO coil's performance *Supercond. Sci. Technol.* **30** 074002

[10] Russenschuck S 2011 *Field Computation for Accelerator Magnets* (Weinheim: Wiley-VCH)

[11] Auchmann B and Russenschuck S 2004 Coil end design for superconducting magnets applying differential geometry methods *IEEE Trans. Magn.* **40** 1208–11

[12] Barth C, Mondonico G and Senatore C 2015 Electro-mechanical properties of REBCO coated conductors from various industrial manufacturers at 77 K, self-field and 4.2 K, 19 T *Supercond. Sci. Technol.* **28** 045011

[13] Fleiter J, Ballarino A, Bonasia A, Bordini B and Richter D 2017 Optimization of Nb_3Sn Rutherford cables geometry for the high-luminosity LHC *IEEE Trans. Appl. Supercond.* **27** 4004305

[14] Wang X, Arbelaez D, Caspi S, Prestemon S O, Sabbi G and Shen T 2017 Strain distribution in REBCO-coated conductors bent with the constant-perimeter geometry *IEEE Trans. Appl. Supercond.* **27** 1–10

[15] Trociewitz U P, Dalban-Canassy M, Hannion M, Hilton D K, Jaroszynski J, Noyes P, Viouchkov Y, Weijers H W and Larbalestier D C 2011 35.4 T field generated using a layer-wound superconducting coil made of (RE)$Ba_2Cu_3O_{7-x}$ (RE = rare earth) coated conductor *Appl. Phys. Lett.* **99** 202506

[16] Matsumoto S, Kiyoshi T, Otsuka A, Hamada M, Maeda H, Yanagisawa Y, Nakagome H and Suematsu H 2012 Generation of 24 T at 4.2 K using a layer-wound GdBCO insert coil with Nb_3Sn and Nb–Ti external magnetic field coils *Supercond. Sci. Technol.* **25** 025017

[17] Richter S C, Ballarino A, Schoerling D, Nes T H, Bernhard A and Müller A S 2022 Progress on HTS undulator prototype coils for compact FEL designs *IEEE Trans. Appl. Supercond.* **32** 4100305

[18] van der Laan D C, Weiss J D and McRae D M 2019 Status of CORC® cables and wires for use in high-field magnets and power systems a decade after their introduction *Supercond. Sci. Technol.* **32** 033001

[19] Wang Z, Li Z, Yu P, Li Z and Wang B 2022 Research status of high temperature superconducting power cable *2022 IEEE Int. Conf. on Electrical Engineering, Big Data and Algorithms (EEBDA)* pp 182–6

[20] Meyer D I and Flasck R 1970 A new configuration for a dipole magnet for use in high energy physics applications *Nucl. Instrum. Methods* **80** 339–41

[21] Kirby G *et al* 2017 Hi-Lumi LHC twin-aperture orbit correctors magnet system optimisation *IEEE Trans. Appl. Supercond.* **27** 1–5

[22] Alonso J, Soleilhavoup A, Wong A, Guiga A and Sakellariou D 2013 Double helix dipole design applied to magnetic resonance: a novel NMR coil *J. Magn. Reson.* **235** 32–41

[23] Quéval L and Gottkehaskamp R 2015 Analytical field calculation of modulated double helical coils *IEEE Trans. Appl. Supercond.* **25** 1–7

[24] Koratzinos M, Kirby G, Van Nugteren J and Bielert E R 2018 A method for greatly reduced edge effects and crosstalk in CCT magnets *IEEE Trans. Appl. Supercond.* **28** 1–5

[25] Do Carmo M P 2016 Differential geometry of curves and surfaces: revised and updated second edition *Dover Books on Mathematics* (Mineola, New York: Dover Publications)

[26] Kreyszig E 1959 *Differential Geometry* (Heritage: University of Toronto Press, Scholarly Publishing Division)

[27] Felcini E, Harray J, Lehtinen T, Perini D, Perez J C, de Rijk G, Dutoit B and Bottura L 2021 Design of the first HTS single-coil demonstrator of gatoroid toroidal gantry for hadron therapy *IEEE Trans. Appl. Supercond.* **31** 4400205

[28] Rosten H I 1973 The constant perimeter end *Technical Report* RL-73-096

[29] Wunderlich W 1962 Über ein abwickelbares Möbiusband *Monatshefte Math.* **66** 276–89

[30] Starostin E L and van der Heijden G H M 2015 Equilibrium shapes with stress localisation for inextensible elastic möbius and other strips *J. Elast.* **119** 67–112

[31] Otten S, Kario A, Kling A and Goldacker W 2016 Bending properties of different REBCO coated conductor tapes and Roebel cables at T = 77 K *Supercond. Sci. Technol.* **29** 125003

[32] van der Laan D C 2009 $YBa_2Cu_3O_{7-\delta}$ coated conductor cabling for low ac-loss and high-field magnet applications *Supercond. Sci. Technol.* **22** 065013

[33] Brouwer L N 2015 Canted-cosine-theta superconducting accelerator magnets for high energy physics and ion beam cancer therapy *PhD Thesis* University of California, Berkely

[34] Prautzsch H *et al* 2002 *Bézier and B-Spline Techniques* (Berlin: Springer)

[35] Horn B K P 1983 The curve of least energy *ACM Trans. Math. Softw.* **9** 441